Ride Blending Control for AWD Electric Vehicle with In-Wheel Motors and Electromagnetic Suspension

Lukas Hott
Technische Universität Ilmenau
Ilmenau, Germany

Valentin Ivanov
Technische Universität Ilmenau
Ilmenau, Germany

Klaus Augsburg
Technische Universität Ilmenau
Ilmenau, Germany

Vincenzo Ricciardi
Technische Universität Ilmenau
Ilmenau, Germany

Miguel Dhaens
DRiV Inc.
Sint-Truiden, Belgium

Monzer Al Sakka
DRiV Inc.
Sint-Truiden, Belgium

Kylian Praet
DRiV Inc.
Sint-Truiden, Belgium

Joan Vazquez Molina
DRiV Inc.
Sint-Truiden, Belgium

***Abstract*—This paper presents a controller for enhancing the ride comfort of electric vehicles with in-wheel motors (IWM) and electromagnetic suspensions (AS). The combined use of IWMs and AS to increase the ride comfort is referred to as Ride Blending (RB). The purpose of this integrated control, its general idea and concept are discussed. The Ride Blending controller is based on a multi-layer hierarchical control architecture. To continuously allocate the demand between the actuators, the control makes use of a cost function optimisation where the ideal control parameters for the current time step are defined. The goal of each component of this function is explained and the structure of each one is described. The use of the ride blending control is then demonstrated on various driving manoeuvres to show the functionality and the ride quality improvement.**

***Index Terms*—electric vehicle, ride blending, in-wheel motor, electromagnetic suspension, ride comfort**

I. Introduction

In-wheel motors (IWM) provide several benefits in terms of vehicle agility and environmental friendliness [1]. However, the consequent increase in unpsrung mass has a detrimental effect on the ride quality. Prior studies show that the vehicle body dynamics is negatively affected in terms of ride comfort [2]. Vehicles with passive suspensions cannot fully compensate the negative aspects of an increased sprung mass, especially with the consideration of conflicting goals such as ride comfort and active safety [3]. A proper solution can be the use of electromagnetic suspension systems, which control the vertical forces between the wheels and the vehicle body.

Many different control strategies of semi-active dampers or electromagnetic suspension elements are intensively developed and have been studied in the past. However, their application to the vertical dynamics problems, caused by IWMs, still needs further research. It should be noted that the purposeful control of IWMs is also capable of generating vertical forces that are comparable to the variation of vertical forces realised by other active chassis systems [4]. The magnitude of the resulting vertical force variation depends heavily on the suspension geometry and achievable torque of the IWMs. With reference to Fig. 1, the main parameters are: (i) the angle between the road and the line from the tyre-road contact point to the instantaneous centre of the wheel caused by compression or deflection of the suspension, which can be called RB-angle, and (ii) the longitudinal force at the tyre-road contact point due to the acceleration or braking of the wheel. Fig. 1 shows the mentioned parameters in a side view of one wheel. The force variation from this effect can be calculated as shown in (1), where the sign depends on the positioning of the instantaneous centre:

$$\Delta F_z = \mp F_x \cdot \tan\varphi, \tag{1}$$

where F_z is the vertical tyre force, F_x is the longitudinal tyre force, φ is the ride blending angle.

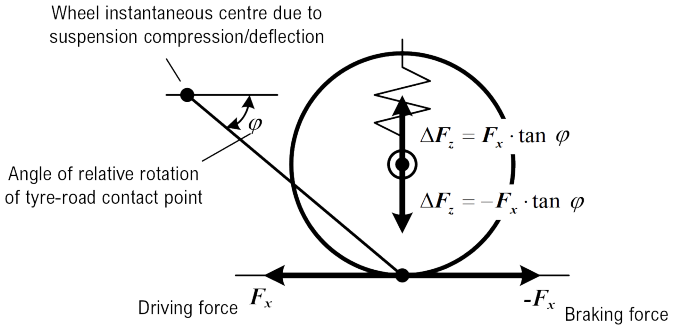

Fig. 1. Side view of a wheel with longitudinal and vertical forces, instantaneous centre of the wheel vertical movement and RB-angle.

Considering general wheel dynamics equation (2)

$$T_w + I_w \cdot \dot{\omega}_w = -F_x \cdot r_{dyn}, \tag{2}$$

where T_w is the wheel torque, I_w is the wheel inertia, ω_w is the wheel rotational velocity, and r_{dyn} is the dynamic tyre

This project has received funding from the European Union's Horizon 2020 research and innovation programme under grant agreement No 824333.

rolling radius, the additional wheel torque for generation of a demanded vertical tyre force $F_{z,dem}$ can be expressed as for the front (f) or rear (r) wheels as follows:

$$T_w^{f,r} = -I_w^{f,r} \cdot \dot{\omega}_w^{f,r} - r_{dyn} \cdot \frac{F_{z,dem}}{\tan \varphi^{f,r}}. \tag{3}$$

The additional torque (3) is added to the torque that is needed for the normal acceleration and braking of the vehicle during a driving manoeuvre.

II. Ride Blending Architecture

The proposed ride blending architecture consists of the hierarchical control with a high-, middle- and low-level controllers as shown in Fig. 2. Thereafter, high- and middle-level controllers are briefly introduced. The low-level controller calculates the real signals, which are used for controlling the actuators. Its detailed description is not presented in this paper.

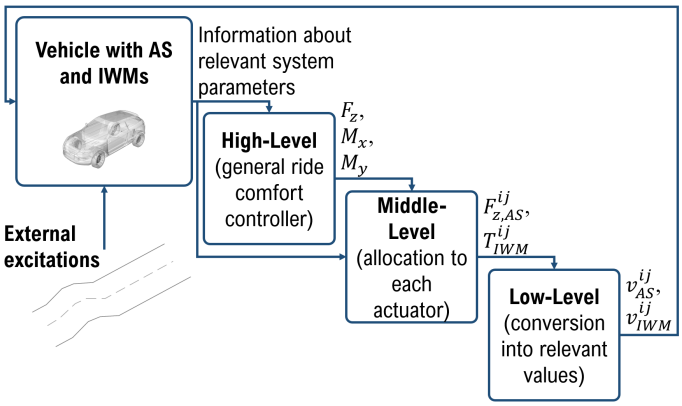

Fig. 2. Hierarchical ride blending control architecture.

A. High-Level Controller

The high-level control defines three virtual variables that have to act on the vehicle body in order to reduce the movement and oscillations of the body: a vertical force F_z, a moment around the x-axis M_x and a moment around the y-axis M_y. The input variables of the high-level controller can be defined as

$$x = \begin{pmatrix} k_s \, \ddot{z}_s \\ k_\phi \, \phi + k_{\dot{\phi}} \, \dot{\phi} \\ k_\theta \, \theta + k_{\dot{\theta}} \, \dot{\theta} \end{pmatrix}, \tag{4}$$

where $\ddot{z}_s$ is the vertical body acceleration, ϕ ($\dot{\phi}$) is the roll angle (roll rate), θ ($\dot{\theta}$) is the pitch angle (pitch rate) and $k_{s,\phi,\theta}$ are corresponding weighting coefficients.

The outputs variables are:

$$v_{HL} = \begin{pmatrix} F_z \\ M_x \\ M_y \end{pmatrix}. \tag{5}$$

These variables have to be allocated to the actuators that are used for the ride blending, which is the task of the middle-level controller.

One simple way to the high-level implementation is to use a PD controller for each input variable. Another promising option would be an Integral Sliding Mode Control, which has been tested in a similar control architecture [3].

B. Middle-Level Controller

The middle-level controller uses the variables v_{HL} to define control variables u for the four AS actuators and for the four IWMs:

$$u = (u_{AS} \quad u_{IWM}), \tag{6}$$

$$u_{AS} = \begin{pmatrix} u_{AS}^{fl} \\ u_{AS}^{fr} \\ u_{AS}^{rl} \\ u_{AS}^{rr} \end{pmatrix} = \begin{pmatrix} F_{z,AS}^{fl} \\ F_{z,AS}^{fr} \\ F_{z,AS}^{rl} \\ F_{z,AS}^{rr} \end{pmatrix}, \tag{7}$$

$$u_{IWM} = \begin{pmatrix} u_{IWM}^{l} \\ u_{IWM}^{r} \end{pmatrix} = \begin{pmatrix} T_{IWM}^{fl} \\ T_{IWM}^{fr} \end{pmatrix} = \begin{pmatrix} -T_{IWM}^{rl} \\ -T_{IWM}^{rr} \end{pmatrix}, \tag{8}$$

where T_{IWM} is the motor torque and the wheels are identified as "fl" for front left, "fr" for front right, "rl" for rear left and "rr" for rear right.

In addition to the control variables allocation, the implemented controller limits vehicle longitudinal acceleration variations, namely the jerk effect, for the sake of driving comfort. In order to do so, a single IWM can not be controlled independently. Conversely, both IWMs on a side of the vehicle shall be controlled together, where one IWM is actuated with $+T_{IWM}^{l/r}$ and the other one with $-T_{IWM}^{l/r}$.

The middle-Level controller uses optimisation (minimisation) of a cost function, where the ideal control parameters u for the current time step have to be defined. For each time step, a number of different values for u are tested and the cost function is calculated for each set of values. The cost function can be described as

$$J_{total} = J_v + J_{P,AS} + J_{P,IWM} + J_s + J_d em. \tag{9}$$

Each component describes a target value, which has to be as low as possible. The perfect values for u can be found by minimising the cost function at each time step:

$$u = min(J_{total}). \tag{10}$$

The components from (9) are explained below.

a) Realisation of the control target from the high-level controller J_v: The difference between the values that result from the current control variables (actual result) and the output of the high-level controller (demand) describes the target of increasing the ride comfort. The bigger the difference, the worse the ride comfort. The actual set of control variables u can be rewritten under for form of matrices as

$$v_{ML} = \begin{pmatrix} F_{z,ML} \\ M_{x,ML} \\ M_{y,ML} \end{pmatrix} = \\ = B_{v,AS} \cdot u_{AS} + B_{v,IWM} \cdot u_{IWM} + C_{v,IWM}, \tag{11}$$

where *"ML"* is for the "middle-level". Then the cost function component is

$$J_v = W_v \| v_{ML} - v_{HL} \| \tag{12}$$

where *"HL"* is for the "high-level" and W_v is a prioritization parameter.

b) Energy demands of actuators $J_{P,AS}$ and $J_{P,IWM}$: The next two components take the theoretical energy demands of the actuators into account. For each actuator, the energy demand is calculated separately and recuperation can be implemented if possible. The parameter W_P is used for scaling and depends on the maximal possible combined energy demand for the actuators.

The energy demand for the active suspension actuators can be calculated as

$$P_{AS} = \frac{F_{z,AS} \cdot v_{AS}}{\eta_{AS}} \; for \; F_{z,AS} \cdot v_{AS} \geq 0 \tag{13}$$

and for recuperation as

$$P_{AS} = F_{z,AS} \cdot v_{AS} \cdot \eta_{AS} \cdot \eta_{reg,AS} \; for \; F_{z,AS} \cdot v_{AS} < 0. \tag{14}$$

where v_{AS} is the actuator speed, η_{AS} is the efficiency of the actuator and $\eta_{reg,AS}$ is the efficiency for recuperation of the actuator.

Then the component $J_{P,AS}$ can be written as

$$J_{P,AS} = W_P \cdot B_{P,AS} \cdot u_{AS}. \tag{15}$$

The energy demand for IWMs can be calculated as

$$P_{IWM} = \frac{T_{IWM} \cdot \omega_{IWM}}{\eta_{IWM}} \; for \; T_{IWM} \cdot \omega_{IWM} \geq 0 \tag{16}$$

and for recuperation as

$$P_{IWM} = T_{IWM} \cdot \omega_{IWM} \cdot \eta_{IWM} \cdot \eta_{reg,IWM} \; for \; T_{IWM} \cdot \omega_{IWM} < 0 \tag{17}$$

where ω_{IWM} is the rotational velocity of the IWM, η_{IWM} is the efficiency of the IWM and $\eta_{reg,IWM}$ is the efficiency for recuperation of the IWM.

The resulting component can be written as

$$J_{P,IWM} = W_P \cdot B_{P,IWM} \cdot u_{IWM}. \tag{18}$$

c) Factor of slip reduction and prevention of critical slip values J_s: This component serves for the reduction of slip to keep the wear of the tire low and for the prevention of critical slip to ensure the active safety. In general this component reduces the control demand of the IWMs if necessary. Its formulation in accordance with [5] can be expressed as follows:

$$J_s = W_s \cdot B_s \cdot u_{IWM} \tag{19}$$

with

$$B_s = \frac{1}{(1 - \frac{s_{res}^l}{s_{res}^{peak}})^{K_s}} \frac{1}{(1 - \frac{s_{res}^r}{s_{res}^{peak}})^{K_s}}. \tag{20}$$

The resulting slip can be calculated with the longitudinal and lateral slip on one wheel. s_{res}^l and s_{res}^r are the maximum resulting slip values on the left and right wheels of the vehicle and s_{res}^{peak} is the current peak resulting slip for maximum tyre contact forces. K_s is a tuning parameter and W_s is used for scaling.

d) Driver demand J_{dem}: The last component takes the driver demand for accelerating and braking into account. It is based on the position of the gas and brake pedal, which range from 0 (not pressed) to 1 (fully pressed). For positions above 0.5, the use of the IWMs get reduced in a way comparable to the component J_s.

$$J_dem = W_{dem} \cdot B_{dem} \cdot u_{IWM} \tag{21}$$

with

$$B_{dem} = (\frac{1}{(1 - Ped)^{K_{dem}}} - \frac{1}{(1 - 0.5)^{K_{dem}}} \\ \frac{1}{(1 - Ped)^{K_{dem}}} - \frac{1}{(1 - 0.5)^{K_{dem}}}), \tag{22}$$

where *Ped* = max (*gas pedal position, brake pedal position*), K_{dem} is a tuning parameter and W_{dem} is used for scaling.

III. Simulation Results

The ride blending controller has been implemented in The Mathworks Inc. Simulink, and the simulations are carried out in IPG CarMaker. The vehicle model describes an electric sport utility vehicle (SUV) with four individual IWMs. In the framework of the simulations, three vehicle configurations are considered: the baseline vehicle features passive suspensions; the AS vehicle is equipped with four electro-magnetic actuators; the RB vehicle enables blended operation of IWMs and AS. Aerodynamic forces, non linear suspension behaviour, a complex model of the electrohydraulic brake system and steering system as well as kinematics and compliance (K&C) parameters are implemented into the vehicle model. The vehicle parameters are listed in Table I. The vehicle model has been experimentally validated in [7].

Three different manoeuvers are tested:

- Sine Sweep with a constant driving speed of 100 km/h and sinusoidal steering with a frequency of 0.5 Hz, the

TABLE I
VEHICLE PARAMETERS

Vehicle type	SUV-class electric vehicle
Wheelbase	2,636 m
Track front	1,628 m
Track rear	1,638 m
CoG height	0,682 m
Total vehicle mass	2045 kg
Unsprung mass front	100,8 kg
Unsprung mass rear	92,8 kg
Tyres	235/55 R 18
Max. torque of IWM	1500 Nm
Max. force of AC actuator	1020 N

steering angle starts at 25° and is increased to 50° over 5 steering periods;
- Random road built up in the simulation environment in accordance with ISO 8606;
- Combined excitations composed from road bumps, a random road and two curves.

Fig. 3, 4 and 5 give examples of the simulation results for one of the tested manoeuvres.

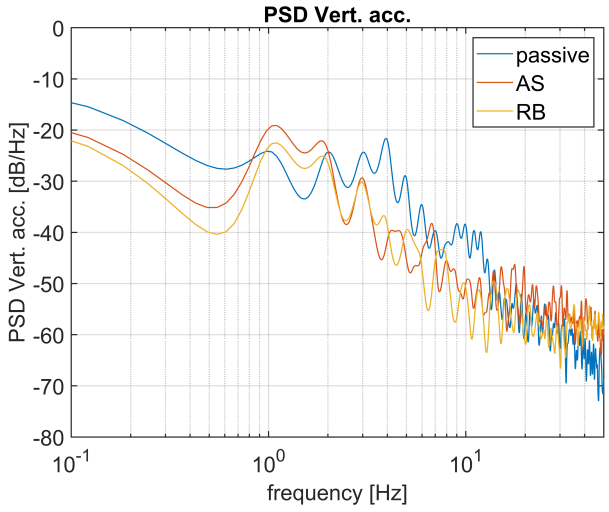

Fig. 3. Example of simulation results for Sine Sweep Manoeuvre: PSD for vertical dynamics.

For the evaluation of the control performance, a Ride Index (RI) is calculated for each variable x (vertical, roll and pitch acceleration):

$$RI_x = \sqrt{\frac{\sum_{f=0Hz}^{20Hz}(w_{fx} \cdot PSD_x)^2}{n}}, \tag{23}$$

where w_{fx} are the weighting coefficients selected in accordance with [6], PSD_x is power spectral density of variable x, n is the number of included elements in the frequency range. In addition to that, the absolute angles are considered (same calculation for θ) with the weighting coefficient k_a:

$$RMS_\phi = \sqrt{\frac{\sum_0^T(\phi(t))^2}{n}} \cdot k_a. \tag{24}$$

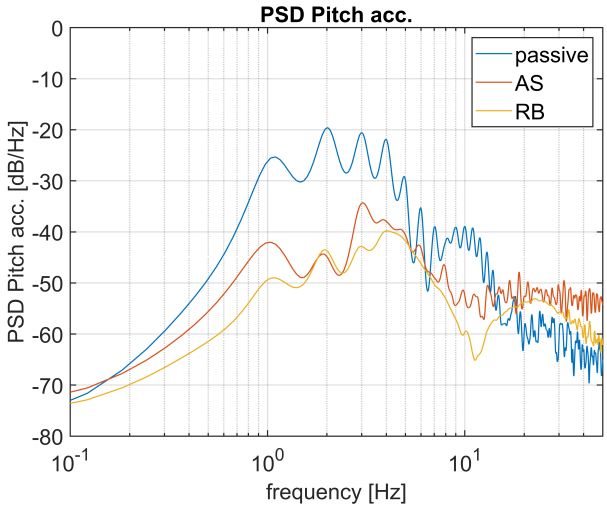

Fig. 4. Example of simulation results for Sine Sweep Manoeuvre: PSD for pitch dynamics.

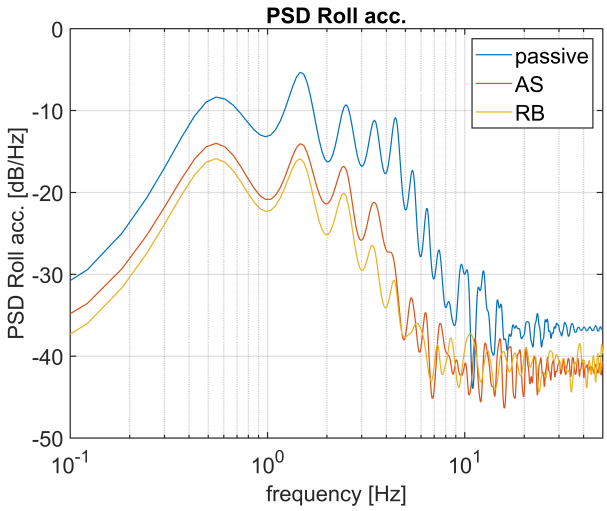

Fig. 5. Example of simulation results for Sine Sweep Manoeuvre: PSD for roll dynamics.

The final RI is calculated as:

$$RI = RI_{\ddot{z}_s} + RI_{\ddot{\phi}} + RI_{\ddot{\theta}} + RMS_\theta + RMS_\phi. \tag{25}$$

The Ride Index should be as low as possible for the best ride comfort. Fig. 6 shows the corresponding simulation results, where the passive suspension system is compared to the AS alone and to the RB system (AS + IWMs). It can be concluded that the simulations with the passive suspension always result in the highest RI, which means that the ride comfort is always worse than the ride comfort with the controlled systems. It can also be seen that the RB control is better than the AS alone in every case.

To show the influence of the different components of the cost function, a combined manoeuvre with lower excitations

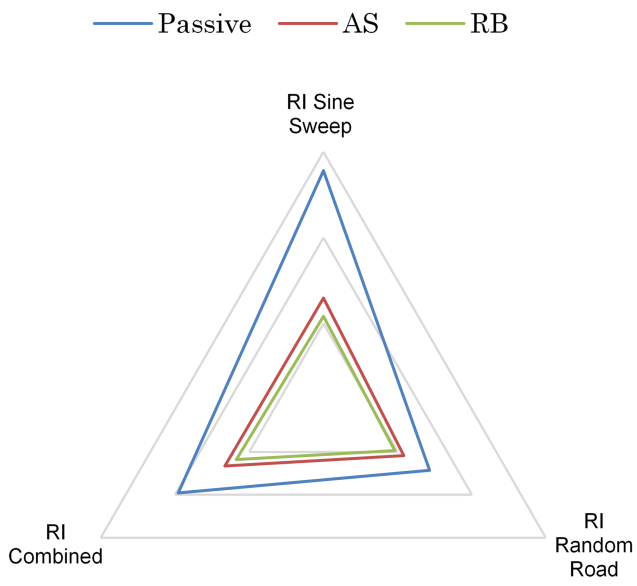

Fig. 6. Comparison of Ride Index for different manoeuvres.

and a brake-in-turn test are simulated as an example. The corresponding results from Table II allows deducing the following conclusions:

- For small control force demands, sole use of AS is preferable because of lower energy consumption and no effect of RB compared to AS;
- For higher control force demands, supportive use of IWMs in addition to the AS is beneficial to match the high-level control demand that leads to the ride comfort improvement with RB control;
- For critical manoeuvres or high driver demand, limitations for controlling the IWMs take place since it brings nearly no effect from RB compared to AS alone.

TABLE II
INFLUENCE OF COST FUNCTION COMPONENTS

Influencing components	Manoeuvre	Effect for RB compared to AS
$J_v, J_{P,AS}, J_{P,IWM}$	Combined with lower excitations	not observed
$J_v, J_{P,AS}, J_{P,IWM}$	Combined with higher excitations	+ 10,2%
J_s, J_{dem}	Brake-in-turn	+ 0,3%

It can further be noted that a sole use of the IWMs can increase the driving comfort in non-critical and small-driver-demand situations up to 50 % compared to the passive system (RI passiv: 0.272, RI IWM alone: 0.128).

IV. CONCLUSIONS

This paper demonstrated the effectiveness of the proposed ride blending control architecture. The combined use of in-wheel motors and active suspensions increases the ride comfort of passenger electric vehicles. The usability of the control and the improvements in terms of ride comfort are shown by means of several driving manoeuvres. Taking the human sensitivity to different vehicle oscillations into account, the ride blending control results in an overall better performance compared to an active suspension alone. Improvements are especially measurable for the vehicle roll movements. In addition, the in-wheel motor control is designed to ensure the active safety and stability of the vehicle.

REFERENCES

[1] S. Murata, “Innovation by in-wheel-motor drive unit,” Vehicle System Dynamics, Vol. 50, pp. 807-830, 2012.
[2] M. Anderson, and D. Harty, “Unsprung mass with in-wheel motors - myths and realities,” Proc. 10th International Symposium on Advanced Vehicle Control, Loughborough, UK, 2010.
[3] A.R. Rojas, H. Niderkofler, and J. Willberger, “Comfort and Safety Enhancement of Passenger Vehicles with In-Wheel Motors,” SAE Technical Paper 2010-01-1146, 2010.
[4] E. Katsuyama, “Decoupled 3D moment control for vehicle motion using in-wheel motors,” SAE Int. J. Passeng. Cars - Mech. Syst., Vol. 6, pp. 137-146, 2013.
[5] R. Wang, H. Karimi, and N. Chen, “Motion control of four-wheel independently actuated electric ground vehicles considering tire force saturations,” Mathematical Problems in Engineering, ID 819302, 2013.
[6] VDI 2057, Human exposure to mechanical vibrations - Whole-body vibration, Blatt 1, Düsseldorf, 2017.
[7] C. Vaseur and S. Van Aalst, “Test Results at Ford Lommel Proving Ground ESR 11 (Version Final),” [Data set]. Zenodo, 2019. http://doi.org/10.5281/zenodo.3263811